Mixing in a T-type Micromixer at High Reynolds Numbers

Andrey V. MINAKOV[1,2*], Valery Ya. RUDYAK[2,3], Andrey A. GAVRILOV[1,2], Alexander A. DEKTEREV[1,2]

* Corresponding author: Tel.: +73912494726 Fax: +73912494726; Email: tov-andrey@yandex.ru
1 Siberian Federal University, Krasnoyarsk, Russia
2 Institute of Thermophysics of SB RAS, Novosibirsk, Russia
3 Novosibirsk State University of Architecture and Civil Engineering, Russia

Abstract Flow regimes and mixing performance in a T-type micromixer at high Reynolds numbers were studied by numerical solution of the Navier–Stokes equations. The Reynolds number was varied from one to one thousand. The cross section of the mixing channel was 100 μm×200 μm, and its length was 1400 μm. The transverse inlet channels were symmetric about the mixing channel, and their cross-section was 100 μm×100 μm, and the total length was 800 μm. Five different flow regimes were identified: (i) stationary vortex-free flow (Re < 5); (ii) stationary symmetric vortex flow with two horseshoe vortices (5 < Re < 150); (iii) stationary asymmetric vortex flow (150 < Re < 240); (iv) nonstationary periodic flow (240 < Re < 400); (v) stochastic flow (Re>400). Maximum mixing efficiency was obtained for stationary asymmetric vortex flow. In this case, an S-shaped vortex structure formed in the flow field. The effect of the slip conditions on the flow pattern and mixing efficiency are studied.

Keywords: Microflow, Micromixers, Microchannels, Transient flow, CFD

1. Introduction

Liquid mixing is an important physical process which is widely used in various microfluidic devices. Since the characteristic flow times are usually extremely small, mixing is accelerated using special devices – micromixers. The operating principles of micromixers and their optimization have been the subject of a great deal of research (see, for example, Tabeling, 2005; Karnidakis et al., 2005; Karnik, 2008; Vanka et al., 2004; Aubina et al., 2005 and references therein). Most papers consider laminar flow at low Reynolds numbers, which are usually characteristic of microflow. In practice, however, situations may arise where Reynolds numbers in microflows are sufficiently large (Mansur et al., 2008; Hoffmann et al., 2006). In addition, micro-channel flow at relatively high Reynolds numbers exhibit a number of interesting new effects, which need to be studied both from a fundamental point of view and for practical purposes.

Various flow regimes in micromixers of this type at high Reynolds numbers have been studied in several papers. Engler et al. (2004) have experimentally demonstrated that there exists a critical Reynolds number at which Dean vortices in a microchannel are no longer symmetric. It has been shown that the critical Reynolds number depends strongly on the channel size. Telib et al. (2004) have numerically studied transitional flow regimes but have not considered mixing processes. Wong et al. (2004) have studied experimentally and numerically the mixing of two liquids at Reynolds numbers from 50 to 1400. Gobert et al. (2006) provided the first numerical evidence for the existence of a nonstationary periodic regime at some Reynolds numbers. The most complete experimental study of mixing in a T-shaped micromixer at moderate Reynolds numbers has been performed by Hoffmann et al. (2006). Velocity and concentration fields in different sections of the mixer were measured using μ-LIF and μ-PIV. Finally, there have been a number of computational and experimental studies (Bothe et al., 2004; 2006; Dreher et al.,

2009) in which some flow regimes in T-shaped microchannels of different cross sections have been calculated, a number of typical flow patterns have been identified, and mixing efficiency has been calculated.
Although flows and mixing in T-shaped micromixers at moderate Reynolds numbers have been studied rather extensively, systematic data on flow patterns and mixing behavior are still not available. The aim of this work is a systematic modeling of flows in T-shaped micromixers. Liquid flow and mixing in micromixers at Reynolds numbers from 10 to 1000 have been studied. The slip conditions on the boundaries are the rather typical for the microflows. Therefore the influence of the slip conditions on flow structure and mixing efficiency are analyzed also.

2. Model and Algorithm

The problem is solved using the Navier-Stokes equations for an incompressible liquid

$$\nabla\cdot(\rho\mathbf{v})=0,$$
$$\partial(\rho\mathbf{v})/\partial t+\nabla\cdot(\rho\mathbf{v}\mathbf{v})=-\nabla p+\nabla\cdot\mathbf{T}, \quad (2.1)$$

where ρ is the liquid density, p is the pressure, $\mathbf{v}$ is the velocity, and $\mathbf{T}$ is the viscous stress tensor. The viscosity of the mixture and its density are given, respectively, by the relations

$$\mu=\sum_i f_i\mu_i, \qquad \rho=\left[\sum_i (f_i/\rho_i)\right]^{-1},$$

where f_i is the mass fraction of component i and μ_i and ρ_i are the partial viscosity coefficient and density. The evolution of the mass fractions is given by the transport equation

$$\frac{\partial\rho f_i}{\partial t}+\nabla\cdot\left(\rho f_i\mathbf{v}\right)=\nabla\cdot\left(\rho D_i\nabla f_i\right), \quad (2.2)$$

where D_i is the diffusion coefficient of molecules of the *i-th* component.
To solve system (2.1) (2.2), we used the algorithm developed in our previous study based on the finite volume method for structured multiblock grids (Rudyak et al., 2008; Gavrilov et al., 2010). Its applicability to microflows was shown in (Rudyak et al., 2010). This work presents the results of simulation of different flow regimes in T-shaped mixers at Reynolds numbers from one to one thousand. The cross section of the mixing channel was 100μm×200μm, and its length was 1400 μm. The transverse inlet channels were symmetric about the mixing channel, their cross-section was 100μm×100μm, and the total length was 800 μm. Clear water was supplied through the left inlet, and water colored with rhodamine dye through the right inlet. The flow rate through the two inlets is the same and equal to Q. The density and viscosity of the two liquids are the same and equal, respectively, to 1000 kg/m^3 and 0.001 Pa·sec. The diffusion coefficient of the dye in water was $D=2.3\cdot10^{-10}$ m^2/s. Thus, the Schmidt number $Sc=\mu/(\rho D)$ for the problem was equal to 3800. This implies that the thickness of the hydrodynamic boundary layer is much greater than the thickness of the diffusion boundary layer, which requires the use of detailed computational grid to resolve the mixing layer. In the calculations, we used a two-block grid consisting of 9.8 million nodes (140 nodes across the width of the mixing channel, 70 along the height, and 1000 along the length). The calculations were performed on the cluster of the Siberian Federal University; 112 cores were used. The run time for the nonstationary flow was about 3 days.
A steady velocity profile was specified at the inlets, and the Neumann conditions (for all scalar quantities, the derivatives normal to the outlet surface are zero) were imposed at the outlet of the mixing channel.
The simulation was performed for various Reynolds number, $\mathrm{Re}=(\rho U d/\mu)$, where $U=Q/(2\rho h^2)$. Here h = 100 μm is the height of the channel and d = 133 μm is the hydraulic diameter.

3. Flow regimes. No-slip conditions

This section discusses the simulation data obtained with no-slip boundary conditions imposed on the walls of the mixer. Several

characteristic flow regimes were identified, which are described below. At low Reynolds numbers (Re < 5), stationary vortex-free flow occurs in the mixer. Increasing the Reynolds number leads to the formation of a pair of stationary symmetric horseshoe vortices at the entrance to the mixing channel, which are commonly called Dean vortices. The horseshoe vortices are due to the development of secondary flows caused by the centrifugal force associated with turning of the flow. The structure of the vortices is shown in Fig. 3.1a. These vortices move along the channel and dissipate. The dissipation mechanism of the vortices is due to viscosity of the liquid, and, therefore, the dissipation rate decreases with increasing Reynolds number. In flow with Re = 120 (see Fig. 3.1b), the horseshoe vortices decay in the mixing channel at distances of about 400 μm from the inlet section, and in flow with Re = 20, at 70 μm. As the Reynolds number increases, the intensity of the Dean vortices also increases and, in addition, their configuration changes (cf. Fig. 3.1a and 3.1b).

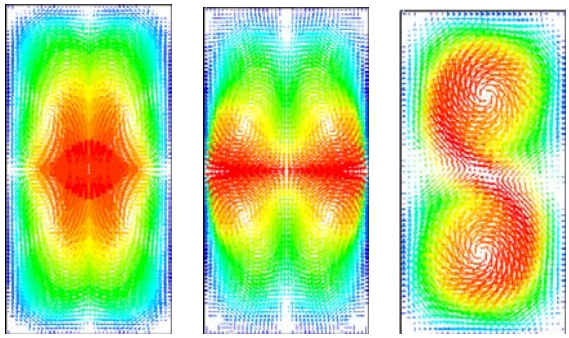

Fig. 3.1. Velocity field in the cross section of the mixing channel at a distance of 100 μm from the entrance for different Reynolds numbers. a) Re = 20; b) Re = 120; c) Re = 186

The occurrence of Dean vortices is a threshold phenomenon, and the corresponding Reynolds number is generally determined by the channel size and can be characterized by the critical Dean number $Dn = \mathrm{Re}\sqrt{d/R}$ (Kelleher, 1980), where R is the radius of curvature of flow turning. In the channel studied in this work, Dean vortices were detected at $Re \approx 20$. In the microchannel considered, the radius of flow turning equal to $R = d/2$ corresponds to a critical Dean number $Dn = 28$.

When the Reynolds number reaches 150, the vortices lose symmetry and rotate by 45^{o} about the central longitudinal plane of the mixer, resulting in the formation of an S-shaped vortex, as shown in Fig. 3.2 left (see also Fig. 3.1c). Here mixing is shown by isolines of dye concentration in four cross sections of the mixer. The first (leftmost) cross section is at the entrance to the mixing channel, the second is at a distance of 100 μm from the entrance, the third at a distance of 200 μm, and the fourth at 400 μm. In the figure, blue corresponds to clear water and red to water tinted with rhodamine. This flow regime is also stationary and is observed up to Reynolds numbers equal to 240.

In the symmetric flow regime (Re <150), the vortices are compensated each other, and the total hydrodynamic momentum was zero. In the asymmetric nonstationary regime, because the vortices in the S-shaped structure rotate in the same direction, the momentum of the flow is different from zero. Naturally, the total mechanical momentum in the system is conserved in both cases because in the asymmetric regime, the compensating momentum arises on the channel walls. Finally it should be noted that the intensity of the vortices in the asymmetric regime is significantly higher than that in the symmetric regime. Therefore, despite dissipation, these vortices are recorded along the entire length of the mixer.

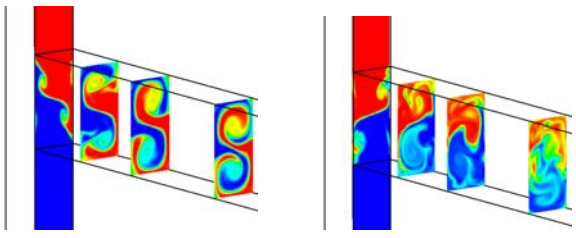

Fig. 3.2. Mixing in micromixer at different Reynolds numbers. Re = 186 (left), Re = 600 (right)

The formation of S-shaped vortices have been experimentally recorded (Hoffmann, 2006).

Fig. 3.3 compares the results of visualization of experiment (Hoffmann, 2006) and our calculation at Re = 186 in three sections of the mixer. The experiment was performed with the same mixer using laser-induced fluorescence (μLIF). In the upper figures, the concentration distribution of the mixing components is shown in the entrance cross section of the mixing channel, in the central figures, at a distance of 1000 μm from the entrance, and in the lower figures, at the exit of the mixer. One can see very good agreement between the shape of the interface of the liquids in the calculation and experiment.

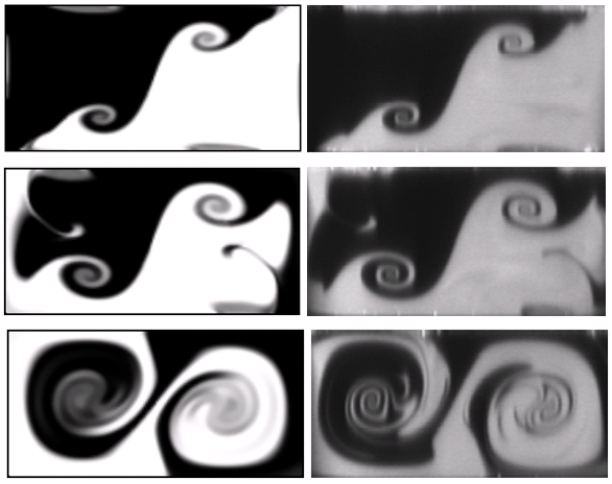

Fig. 3.3. Isolines of dye concentration in different cross sections of the mixer for Re = 186. a) calculated results, b) experimental data (Hoffmann, 2006)

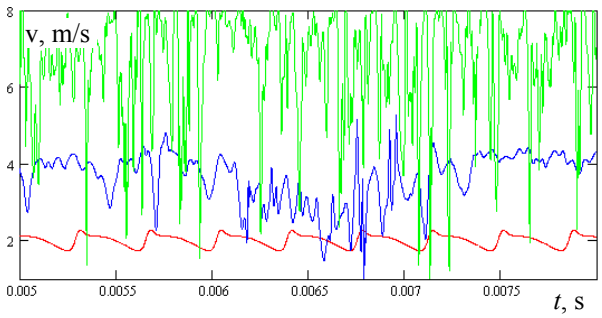

Fig. 3.4. The flow velocity versus time (sec) at the mixer exit

The stationary asymmetric flow regime described above is observed in the range of Reynolds numbers from 150 to 240. Starting at a Reynolds number approximately equal to 240, the flow ceases to be stationary. In the range of Reynolds numbers 240 < Re < 400, a periodic flow regime occurs. This means that the flow velocity is also a periodic function of time. In Fig. 3.4, this flow regime corresponds to the lower red curve. The oscillation frequency of the flow f is determined by many factors, such as channel geometry, liquid viscosity, and Reynolds number. To describe this dependence, we introduce the Strouhal number $St = (fd^2)/(\nu \mathrm{Re})$, which is actually the dimensionless frequency of flow oscillations normalized by the Reynolds number (ν is the kinematic viscosity). A diagram of the Strouhal number versus Reynolds number is shown in Fig. 3.5 (squares). The oscillation frequency increases monotonically to Re = 300 and then slightly decreases. The data of our calculations are in good agreement with experimental results Dreher et al. (2009), which in Fig. 3.5 are marked with red tags. Maximum differences are observed at high Reynolds numbers, but it should be noted that the experimental data were obtained for a channel with cross-sectional dimensions of 600μm× 300μm.

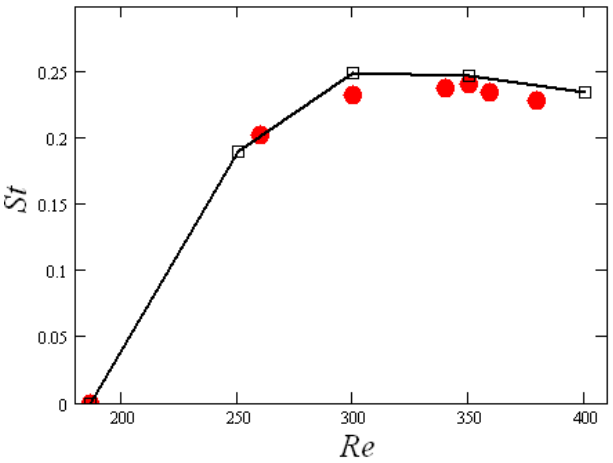

Fig. 3.5. Strouhal number versus Reynolds number

Starting at a Reynolds number of about 450, the strict periodicity of the oscillations of the flow is lost. The flow becomes first quasi-periodic and then chaotic (Re > 600). In the latter case, the frequency spectrum becomes almost continuous. This can be clearly seen in Fig. 3.4, where the blue curve corresponds to a Reynolds number of 600, and the green curve

to a Reynolds number of 1000.

The frequency distribution of the kinetic energy of the flow pulsations for Re = 600 is shown in Fig. 3.6. This spectrum was obtained for the point at the center of the mixing channel at a distance of 400 μm from the entrance. The dotted straight line in the figure corresponds to the Kolmogorov–Obukhov universal law. Although for Re = 600, the spectrum cannot be considered completely continuous, as in the case of developed turbulent flow, it nevertheless contains a large number of frequencies and an inertial interval, which at least suggests a transitional flow regime. This early (for channel flows) transition to turbulence is due to Kelvin–Helmholtz instability in the entrance section of the mixing channel. Nevertheless, calculations show that if the mixing channel is long enough, then, with increasing distance from the site of confluence of the flows, the pulsations gradually fade, the flow becomes laminar, and a steady laminar velocity profile is established.

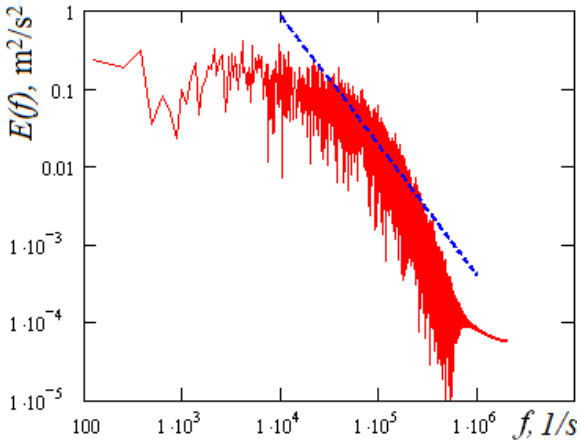

Fig. 3.6. Spectrum of the kinetic energy of velocity fluctuations for Re = 600

Figure 3.7 shows the friction coefficient of the mixing channel as a function of Reynolds number for this mixer. The friction coefficient was determined by the following formula $\lambda = (2\Delta P d)/(\rho U^2 L)$, where ΔP is the pressure drop along the channel and L is its length. Red circles and the line connecting them correspond to calculations. For comparison with the calculated data, the dashed line in the figure shows the friction coefficient for stationary laminar flow in a rectangular channel with an aspect ratio of 0.5. In this case, the friction coefficient is close to 64/Re (green dotted line). An analysis shows that for low Reynolds numbers, the friction coefficient in the micromixer is on average 20–30% higher than the friction coefficient for stationary flow. For Reynolds numbers Re > 150, the friction coefficient sharply deviates from the relation λ = 64/Re, which also indicates laminar-turbulent transition. For the turbulent regime, the calculated values of the friction coefficient in the micromixer is well described by the relation $\lambda = 1.8/\mathrm{Re}^{0,25}$. This is 5.68 times higher than the classical Blasius relation ($\lambda = 0.316/\mathrm{Re}^{0,25}$) for developed turbulent flow in a straight channel. This large difference is due to the flow turning at the entrance to the channel and flow swirling in the mixing channel.

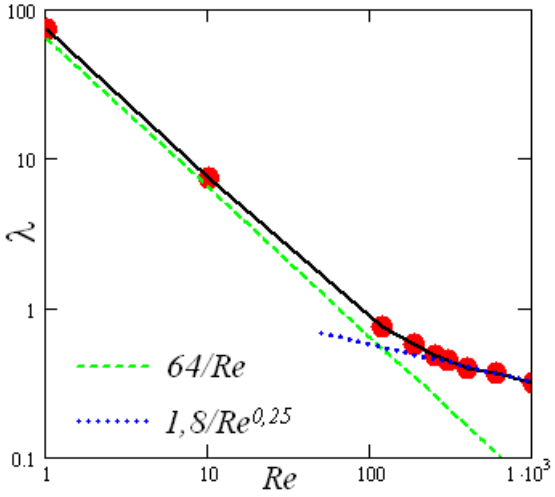

Fig. 3.7. Friction coefficient versus Reynolds number in the mixing channel

4. Mixing Efficiency

At high Reynolds numbers, the flow and mixing are substantially three-dimensional. In this case, the mixing efficiency is conveniently described by the parameter $M = 1 - \sqrt{\sigma/\sigma_0}$, where

$$\sigma = \frac{1}{V}\int_V \left(f - \bar{f}\right)^2 dV$$

and σ_0 is the dispersion maximum, $\bar{f}$ is the value of concentration of full mixing ($\bar{f}$ =0.5).

As noted above, at low Reynolds numbers (Re < 5), stationary vortex-free flow occurs in the mixer. Mixing in this case is due to ordinary molecular diffusion and its efficiency is rather low (about 3%, see Fig. 4.1) (Rudyak et al., 2010). Increasing the Reynolds number leads to the formation of stationary Dean vortices. These horseshoe vortices are symmetric about the central longitudinal plane of the mixer. Each of these vortex horseshoes is within the same liquid and does not cross the interface between the liquids being mixed, so that this interface remains almost flat. Since the diffusion Peclet number increases with increasing Reynolds number, the mixing efficiency in this case even decreases compared with mixing in vortex-free flow (see Fig. 4.1), and remains low up to Reynolds numbers of about 150.

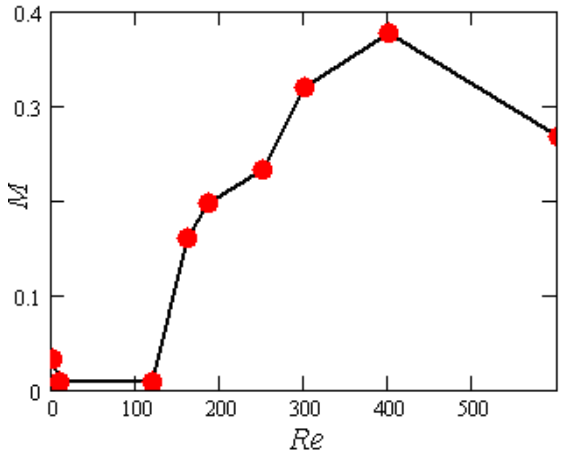

Fig. 4.1. Mixing efficiency versus Reynolds number

The loss of symmetry of the Dean vortices and the formation of the S-shaped vortex structure lead to a qualitative change in the mixing pattern. The contact surface of the mixing liquids increases significantly, resulting in a considerable increase in the mixing efficiency (see Fig. 4.1). As the flow pattern changes from symmetric (Re < 150) to nonsymmetric (Re > 150), the mixing efficiency increases by a factor of 25.

The transition to turbulence leads to the breakdown of the S-shaped vortex structure which was formed in the mixing channel at Re > 150 and existed in the nonstationary regime (see Fig. 3.2 (right), which shows the evolution of the S-shaped vortex structure for Re = 600). The flow breaks up into a set of fairly large vortices. This results in a reduction in the contact area of the mixed liquids and a sharp decrease in the mixing efficiency (M = 26 % at Re = 600). Naturally, with a further increase in the Reynolds number, the large-scale vortex structures break down into many smaller vortices, which provide very good mixing of the flow. The mixing efficiency in the developed turbulent flow will be substantially higher than the laminar value.

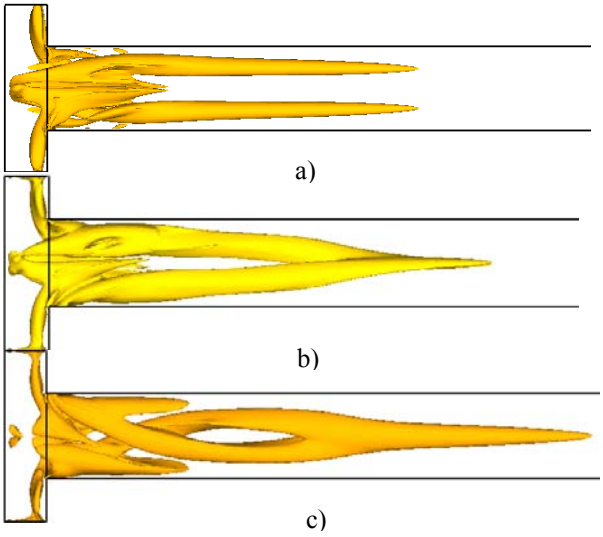

Fig. 5.1. Flow vortex structure in microchannel at various value of the slip length *b*. Re = 186. a) *b* = 0; b) *b* = 10 μm; c) *b* = 30 μm

5. Flow regimes. Slip conditions

The channel length of the mixers should be sufficiently great to provide flow mixing. Naturally, this leads to a significant pressure drop due to friction on the channel walls. On the other hand, it is obvious that such losses are much lower in the case of flow slip rather than no-slip conditions on the channel walls. In microflows the slip length can reach a few hundred nanometers or even tens of microns. To increase the slip length the various hydrophobic or even ultrahydrophobic coatings is used (Ou et al., 2004; Lauga et al., 2005). In this case, the slip length can reach

tens of micrometers. Applying the hydrophobic coatings in microchannels we can significantly decrease the pressure drop. The mixing efficiency is not practically changed in flows with low Reynolds numbers (Rudyak et al., 2010) because the flow structures with no-slip or slip conditions are the similar. However the situation is changed in flows with moderately Reynolds numbers. The main conclusion is the following. The flow structure is not practically changes at small and moderately slip lengths (up to 5 μm). However, the flow structure at moderately Reynolds numbers is considerably changed at large slip lengths.

In Fig. 5.1 the flow structure is shown by means of the iso surface of value λ_2 (λ_2 is the second eigenvalue of tensor $\mathbf{S}:\mathbf{S}+\mathbf{\Omega}:\mathbf{\Omega}$, here $\mathbf{S}$ and $\mathbf{\Omega}$ are stress tensor and vorticity tensor respectively). As we mentioned above the two-vortices structure is formed in the mixer flow field at zero slip length (see Fig. 5.1a). But this structure is transformed to a single whole vortex at large slip length (see Fig. 5.1b and 5.1c). Naturally the mixing efficiency grows also when the slip length increases. This growth is about 30 % for the mixer presented in Fig. 5.1. On the other hand the pressure drop decreases monotonically if the slip length increases (about 30–40 % for mixers presented in Fig. 5.1).

Conclusions

So, we can define the following specific regimes of flows in T-type micromixer with no-slip boundary conditions.

- Stationary vortex-free flow (Re < 5);
- Stationary symmetric vortex flow with two symmetric horseshoe vortices form at the entrance of the mixer (5 < Re < 150);
- Stationary asymmetric vortex flow occurs in the mixer (150 < Re < 240). The horseshoe vortices formed at the entrance lose symmetry and rotate by 45 degrees to the central longitudinal plane of the mixer;
- Nonstationary periodic flow (240 < Re < 400);
- Practically stochastic regime (400 < Re < 1000). The S-shaped vortex structure observed at lower Reynolds numbers is destroyed.

Using the slip boundary conditions (hydrophobic skins) we get possibility to change this regimes. The flow structure and mixing efficiency will be appreciably modified if the inlet conditions are non-symmetric. This regimes modification may be used to control the fluids mixing.

Acknowledgments

This work was supported in part by the Russian Foundation for Basic Research (Grant No. 10-01-00074) and the Federal Special Program “Scientific and scientific-pedagogical personnel of innovative Russia in 2009-2013” (projects No. P230, No. 14.740.11.0579 and No. 14.740.11.0103).

References

Aubina, J., Fletcherb, D.F., and Xuereb, C., 2005. Design of micromixers using CFD modeling. Chem. Eng. Sci. 60, 2503–2516.

Bothe, D., Stemich, C., and Warnecke, H.-J., 2004. Theoretische und experimentelle Untersuchungen der Mischvorgänge in T-förmigen Microreaktoren. Teil 1. Numerische Simulation und Beurteilung des Strömungsmischens. CIT. 76, 1480–1484.

Bothe, D., Stemich, C., and Warnecke, H.-J., 2006. Fluid mixing in a T-shaped micro-mixer. Chemical Engineering Science. 61, 2950 – 2958.

Dreher, S., Kockmann, N., and Woias, P., 2009. Characterization of laminar transient flow regimes and mixing in T-shaped micromixers. Heat Transfer Engineering, 30, 91–100.

Engler, M., Kockmann, N., Kiefer, T., and Woias, P., 2004. Numerical and experimental investigations on liquid mixing in static micromixers. Chem. Eng. J. 101, 315–322.

Gavrilov, A.V., Minakov, A.V., Dekterev A.A., and Rudyak, V.Ya., 2010. Numerical algorithm for simulating

laminar flows in an annular channel with eccentricity. Sib. Zh. Industr. Matem. 13(4), 3–14.

Gobert, C., Schwert, F., and Manhart, M., 2006. Lagrangian scalar tracking for laminar micromixing at high Schmidt numbers. In book: Proc. ASME Joint U.S.-European Fluids Eng. Summer Meeting. Miami.

Hoffmann, M., Schluter, M., and Rubiger, N., 2006. Experimental investigation of liquid–liquid mixing in T-shaped micro-mixers using μ-LIF and μ-PIV. Chemical Engineering Science. 61 2968–2976.

Jiménez, J., 2005. The growth of a mixing layer in laminar channel. J. Fluid Mech. 535, 245–254.

Karnidakis G., Beskok A., Aluru N., 2005. Microflows and nanoflows. Interdisciplinary Applied Math. V. 29. Springer Science+Business Media, Inc.

Karnik, R., 2008. Microfluidic mixing. In book: Encyclopedia of microfluidics and nanofluidics. Ed. Li D. Springer. P. 1177–1186.

Kelleher, M.D., Flentie, D.L., and McKee, R.J., 1980. An experimental study of the secondary flow in a curved rectangular channel. Transactions J. Fluids Engineering. 102, 92–96.

Lauga, E., Brenner, M.P., and Stone, H.A., 2005. Microfluidics: the no-slip boundary condition. In book: Handbook of experimental fluid dynamics. Eds. Foss J., Tropea C., and Yarin A. Ch. 15.

Mansur, E.A., Mingxing, Y.E., Yundong, W., and Youyuan, D, 2008. A state-of-the-art review of mixing in microfluidic mixers. Chinese J. Chemical Eng. 16(4), 503–516.

Ou, J., Perot, B., and Rothstein, P., 2004. Laminar drag reduction in microchannels using ultrahydrophobic surfaces. Phys. Fluids. 16, 4635–4643.

Rudyak, V.Ya., Minakov, A.V., Gavrilov, A.A., and Dekterev, A.A., 2008. Application of new numerical algorithm of solving the Navier–Stokes equations for modeling the work of a viscometer of the physical pendulum type. Thermophysics & Aeromechanics. 15, 33–345.

Rudyak, V.Ya., Minakov, A.V., Gavrilov A.V., and Dekterev A.A., 2010. Simulation of flows in micromixers. Thermophysics & Aeromechanics. 17, 565–576.

Tabeling, P., 2005. Introduction to microfluidics. Oxford University Press.

Telib, H., Manhart, M., and Iollo, A., 2004. Analysis and low-order modeling of the inhomogeneous transitional flow inside a T-mixer. Phys. Fluids. 16, 2717–2731.

Vanka, S.P., Luo, G., and Winkler, C.M., 2004. Numerical study of scalar mixing in curved channels at low Reynolds number. AIChE J. 50, 2359–2368.

Wong, S.H., Ward, M.C.L., and Wharton, C.W., 2004. Micro T-mixer as a rapid mixing micromixer. Sens. & Act. B. 100, 359–379.